

Experimental and Post-Test Calculation Results of the Integral Reflood Test QUENCH-12 with a VVER-type Bundle

J. Stuckert¹, J. Birchley², M. Große¹, T. Haste², L. Sepold¹, M. Steinbrück¹

¹Forschungszentrum Karlsruhe, Hermann-von-Helmholtz-Platz 1, D-76344 Eggenstein-Leopoldshafen, Germany
Tel: (+49) 7247 82 2558, Fax: (+49) 7247 82 2095, Email: juri.stuckert@imf.fzk.de

²Paul Scherrer Institute, CH-5232 Villigen PSI, Switzerland

Abstract – The QUENCH-12 experiment was carried out to investigate the effects of VVER materials (niobium-bearing alloys) and bundle geometry on core reflood, in comparison with test QUENCH-06 using western PWR materials (Zircaloy-4) and bundle geometry. While the PWR bundle uses a single unheated rod, 20 heated rods, and 4 corner rods arranged on a square lattice, with a heated length of 1000 mm, the VVER bundle uses 13 unheated rods, 18 heated rods and 6 corner rods, arranged on a hexagonal lattice. The test was conducted at the Forschungszentrum Karlsruhe on 27 September 2006 with largely the same protocol as QUENCH-06, in order to demonstrate the effects on the VVER characteristics more readily. The test protocol involved pre-oxidation to a maximum of about 200 µm oxide thickness at a temperature of about 1200 °C, followed by a power ramp until a temperature of 1800 °C was reached, then reflood with water at room temperature was initiated. The total hydrogen production was 58 g (QUENCH-06: 36 g), 24 g of which were released during reflood (QUENCH-06: 4 g). Reasons for the increased hydrogen production may be extensive damaging of the cladding surfaces due to the breakaway oxidation and local melt formation with subsequent melt oxidation, due perhaps to slightly extended pre-quench transient. Post-test videoscope observations and metallographic investigations showed an influence of the breakaway oxidation with extensive spalling of oxide scales of rod claddings, shroud and auxiliary corner rods. The hydrogen content in the corner rods, withdrawn from the bundle during the test, reached more than 30 at% at the bundle elevations of 850 and 1100 mm. Post-test calculations were performed with local versions of SCDAP/RELAP5 (S/R5) following on from pre-test analyses with S/R5 and SCDAPSIM. A variety of oxidation models were used (Cathcart-Pawel, Sokolov, Urbanic-Heidrick and Prater-Courtright) to investigate the observed differences between the QUENCH-12 and QUENCH-06 oxidation behaviour.

I. INTRODUCTION

The purpose of the QUENCH experiments performed at the Forschungszentrum Karlsruhe (FZK) is to investigate the hydrogen source term resulting from the water or steam injection into an uncovered core of a light water reactor (LWR), to examine the physicochemical behaviour of overheated fuel elements under different flooding/cooling conditions, and to create a database for model development and code improvement. The physical and chemical phenomena of the hydrogen release are not sufficiently well understood. In particular, an increased hydrogen production during quenching cannot be determined on the basis of the available Zirconium alloy/steam oxidation correlations. Presently it is assumed that the following phenomena lead to an enhanced oxidation and hydrogen generation: cracking and spalling of surface oxide layer, steam starvation conditions prior to

quenching, and melt oxidation. In most of the code systems describing severe fuel damage, these phenomena are either not considered or only modeled in a simplified empirical manner.

The QUENCH-12 experiment¹ was carried out to investigate the effects of VVER materials (niobium-bearing alloys) and bundle geometry on core reflood, in comparison with test QUENCH-06 using western PWR materials (Zircaloy-4) and geometry². The test protocol was based on numerous calculations with SCDAP/RELAP5, SCDAPSIM, and ICARE/CATHARE, with adaptation being based on the QUENCH-12 pre-test with short-time bundle heating to 800 °C. The main test was conducted with similar protocol to QUENCH-06, so the effects on the VVER characteristics could be observed more easily.

II. TEST FACILITY AND INSTRUMENTATION

In the forced-convection mode of the test facility, superheated steam from a steam generator and superheater together with argon as a carrier gas for gas measurements enter the test bundle at the bottom (Fig. 1). The argon, the steam not consumed, and the hydrogen produced in the zirconium-steam reaction flow from the bundle outlet at the top through a water-cooled off-gas pipe to the condenser where the steam is separated from the non-condensable gases. The system pressure in the test section is around 0.2 MPa. The test section has a separate inlet at the bottom to inject water for reflood.

The test bundle is approximately 2.5 m long and is made up of 18 heated and 13 unheated fuel rod simulators (Fig. 2). Heating is electric by 4 mm diameter tungsten heaters installed in the rod center, and the heated length is 1.024 m.

Electrodes of molybdenum/copper are connected to the tungsten heaters at one end and to the cable leading to the DC electrical power supply at the other end. The distribution of the electric power within the two groups is as follows: 33 % of the power is released in the six inner fuel rod simulators, 67 % in the twelve outer fuel rod simulators.

The tungsten heaters of heated rods are surrounded by annular ZrO_2 pellets. The center hole of the unheated rods was used for installation of centerline thermocouples.

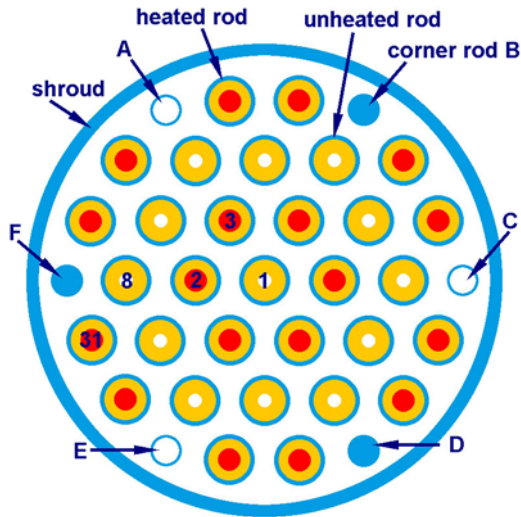


Fig. 2. Bundle cross-section with marked rods.

The rod cladding of the fuel rod simulator is identical to that used in VVERs with respect to material and dimensions ($Zr1\%Nb$ (E110), 9.13 mm outside diameter, 0.7 mm wall thickness). The fuel rod simulators are held in position by seven grid spacers all made of $Zr1\%Nb$.

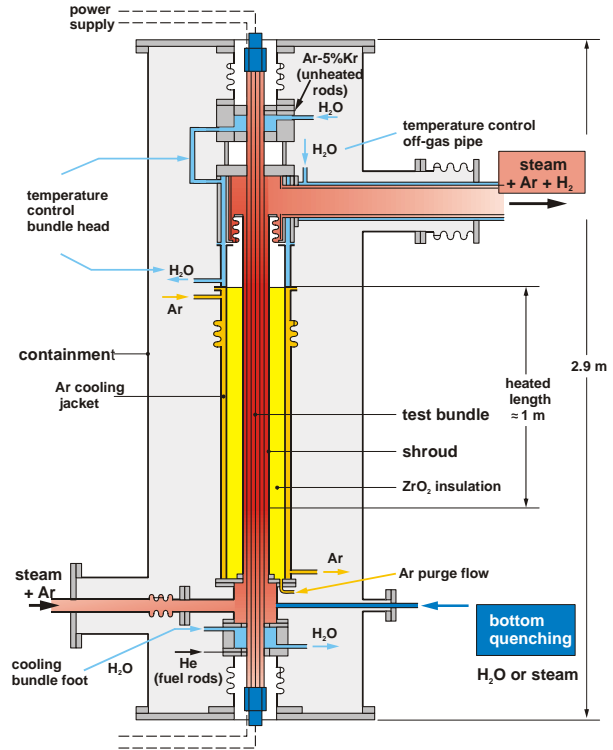


Fig. 1. QUENCH test section with test bundle and fluid lines.

Heated and unheated test rods, including the central one, are filled with $Ar5\%Kr$ and He , respectively, at a pressure of approx. 0.22 MPa. The different fill gases allow observation of a first cladding failure which then can be distinguished between heated and unheated test rods.

There are six $Zr1\%Nb$ corner rods installed in the bundle. Three of them, i.e. rods "A", "C", and "E" are made of a solid $Zr1\%Nb$ rod at the upper part and a $Zr1\%Nb$ tube at the lower part and are used for thermocouple instrumentation whereas the other three corner rods, i.e. rods "B", "D", and "F", are made of solid $Zr1\%Nb$ rods of 6 mm diameter and can be withdrawn from the bundle to check the amount of ZrO_2 oxidation at pre-defined times.

The test bundle is surrounded by a shroud of $Zr2.5\%Nb$ (E 125) with a 37 mm thick ZrO_2 fiber insulation extending from the bottom to the upper end of the heated zone and a double-walled cooling jacket of stainless steel over the entire length. The shroud tube has an outer diameter of 88 mm and a wall thickness of 2.25 mm.

The annulus between shroud and cooling jacket is filled with stagnant argon of 0.22 MPa. The 6.7 mm annulus of the cooling jacket is cooled by an argon flow. The absence of ZrO_2 insulation above the heated region and the water cooling of the bundle head are to avoid overheating in that region of the bundle.

The test section has a coolant flow area of 32.8 cm² and a hydraulic diameter of 10.4 mm and is instrumented with thermocouples attached to the cladding, the shroud, and the cooling jackets at elevations between -0.250 and 1.350 m. The thermocouples attached to the outer surface of the rod cladding at elevations as well between -0.25 and 1.35 m are designated "TFSH" for the heated rods and "TFSU" for the unheated ones, including the central rod. The thermocouples "TFC" installed in the center of the unheated rods are isolated from the steam flow through the bundle.

The thermocouples of the hot zone, i.e., from 0.650 m upward, are high-temperature thermocouples with W-5Re/W-26Re wires, HfO₂ insulation, and a duplex sheath of tantalum (internal)/zirconium with an outside diameter of 2.1 mm. Up to the 0.55-m elevation, NiCr/Ni thermocouples (1 mm diameter, SS cladding, MgO insulation) are used for temperature measurements of rod cladding and shroud. In addition, one centerline thermocouple each was mounted inside three corner rods designated "TIT." All three thermocouples TIT C/11, TIT E/12 and TIT A/13 at 0.75, 0.85 and 0.95 m, respectively, were of the high-temperature type.

The hydrogen is mainly analyzed by a mass spectrometer Balzers "GAM300" located at the off-gas pipe of the test facility. Another H₂ analyzer located downstream from the condenser was installed as a backup instrument.

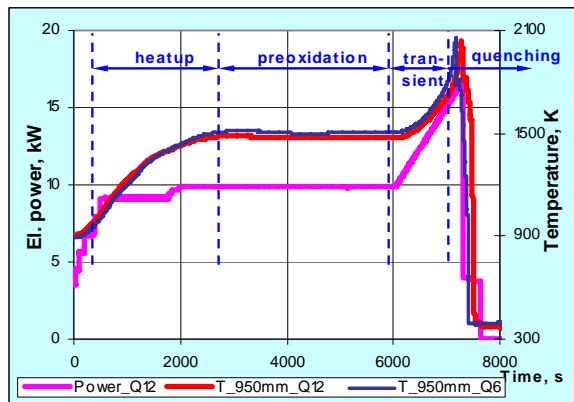


Fig.3. Temperature at the 0.95 m level (Q12: TFC 1/13; Q6: TIT A/13) and electric power vs. time together with an indication of the QUENCH-12 test phases.

III. TEST CONDUCT

The main test phases of the QUENCH-12 experiment are shown in Fig. 3 and summarized below.

- Phase I Stabilization at ~620 °C. Facility checks.
- Phase II Heatup by ~0.3-0.7 K/s to ~1200 °C for ~48 min (first transient).
- Phase III **Pre-oxidation** in a flow of 3.3 g/s of superheated steam and 3.3 g/s argon for ~53 min at a relatively constant temperature of ~1200 °C.
- Phase IV **Transient** heatup from ~1200 to 1800 °C with a heating rate of ~0.3-2.5 K/s for 20.5 min.
- Phase V **Quenching** of the bundle from the bottom by a water flow of 48 g/s.

Pre-oxidation of the bundle was carried out to achieve the target cladding oxidation of around 200 μm at the upper end of the heated zone. The first corner rod D, which was withdrawn at the end of the pre-oxidation phase, revealed an extensive breakaway oxidation along the complete hot zone. It was not possible to measure the oxide layer thickness due to spalling of the oxide scales (Fig. 4). The second corner rod F was withdrawn during the transient phase before starting the moderate temperature escalation. This rod also exhibited an extensive spalling of oxide scales.



Fig. 4. The withdrawn corner rods D (lower) and F (upper) revealed breakaway oxidation with intensive spalling of oxide scales.

The power was ramped after pre-oxidation at a rate of 5.1 W/s in order to increase the temperature until the desired maximum temperature of 1800 °C before quench was reached. The axial temperature distributions given in Fig. 5 for three different times before reflood show that the hottest bundle zone was located between 0.85 and 1.05 m.

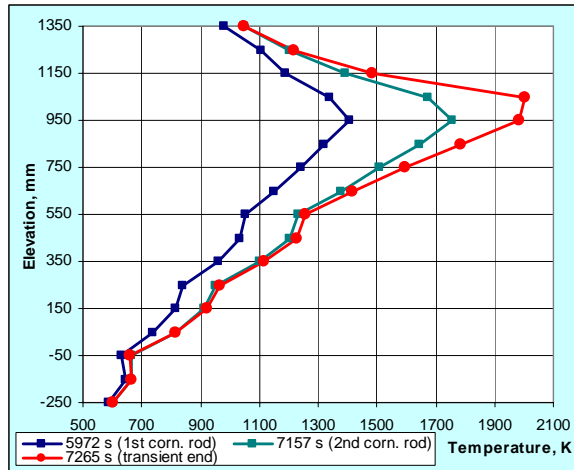


Fig. 5. Axial temperature profiles during pre-oxidation and transient phases.

Then, reflood with 48 g/s of water at room temperature was initiated starting with a rapid filling of the lower plenum of the test section. The electrical power was reduced to 4 kW during the reflood phase, thus approximating effective decay heat levels. Following the initiation of reflood, a moderate temperature excursion of about 50 K was observed for 15 s, i. e. over a longer period than in QUENCH-06. Some temperatures exceeded for a short period the melting point of the β -Zr before reflood (2033 K, Fig. 6).

Shroud failure was detected by a sharp decrease of pressure in the annulus between shroud and cooling jacket at around the initiation of reflood, while heated and unheated rods failed practically simultaneously towards the end of the transient phase. Rod failures were detected by the mass spectrometer with releases of Kr and He, which were used for filling the heated and unheated rods respectively.

IV. BREAKAWAY OXIDATION

The third corner rod, i. e. rod B, was pulled after the test. The surface of the rod had the typical breakaway structure with the partially spalled oxide layer similar to corner rods D and F withdrawn earlier. The maximum thickness of not-spalled oxide layer of about 500 μm was measured for corner rod B at elevation 0.88 m. The thickness of the corresponding α -Zr(O) layer was about 650 μm . The internal β -Zr zone of this corner rod relocated at this bundle elevation due to melting.

The visual survey of the bundle showed that some part of the β -Zr on the outer shroud surface was partially molten at elevations between 0.85 and 1.05 m and reacted with the ZrO_2 heat insulation. The shroud ruptured at these elevations and the upper shroud part was removed from the bundle during dismounting.

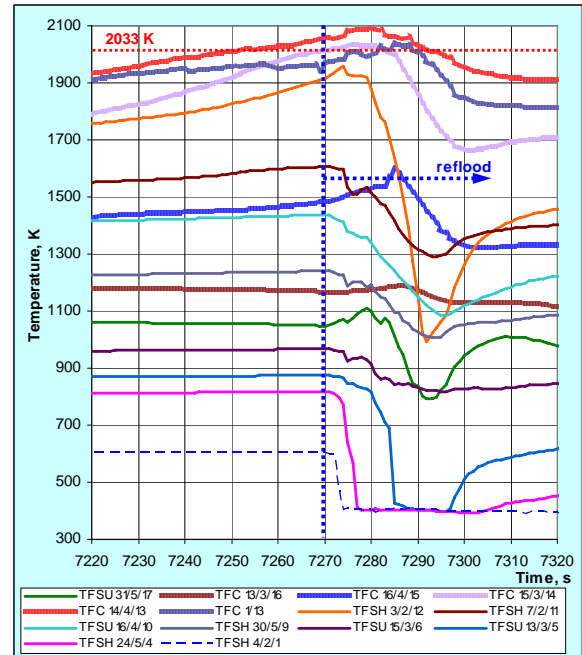


Fig. 6. Selected readings of bundle thermocouples between elevations 1 (-0.25 m) and 17 (1.35 m). Marking of thermocouples: rod number/rod group/elevation.

The rod surface was intensively oxidised along this hot region. Some simulator rods had circumferential cracks resulting in breaches. It is interesting to note that the surface of the rod claddings showed more regular and homogeneous structure of the oxide layer than the surface of the solid corner rods. Both surfaces show breakaway oxidation being more pronounced at the corner rods. One possible reason for it could be the different mechanical properties of cladding tubes and solid corner rods. Another possible reason could be the different initial rod surface quality³: the surface of corner rods is coarser in comparison with the anodised surface of fuel rod cladding.

The QUENCH-12 bundle was investigated in detail by videoscope before filling with epoxy resin. As the metallographic investigation of the epoxy filled bundle is a selective 2-D method, the videoscope allows continuous 3-D observations. Scanning by the videoscope camera at the positions of withdrawn corner rods revealed differences in the surface morphology. The lowest elevation where breakaway oxidation of cladding surface took place was at 0.40 m (Fig. 7). The maximum temperature at this bundle position was about 850 $^{\circ}\text{C}$.

The spalled oxide scales were partially removed by pull-out of the videoscope from the bundle. The videoscope was re-inserted with a side view camera lens at the same axial position of corner rod channel D showing formation of regular dark oxide layer under the spalled oxide scales (Fig. 8).



Fig. 7. Videoscope observation at bundle elevation 0.40 m at the empty position of corner rod F: circumferential spalling of the oxide layer on the surface of fuel rod simulator cladding.

The formation of typical breakaway oxidation at the relatively cooler shroud took place at higher elevations. The initially coarse shroud surface revealed thicker spalled oxide scales, but the oxide sub-layer showed also the regular dark structure (Fig. 9). The inner shroud surface showed at the higher hottest elevations a nodular kind of breakaway oxidation, whereas there is no evidence of breakaway on the cladding surface at these elevations (Fig. 10). However the formation of longitudinal and circumferential cladding cracks in the hot bundle zone (0.70-1.00 m) is typical for Zircaloy-4 cladding as well.

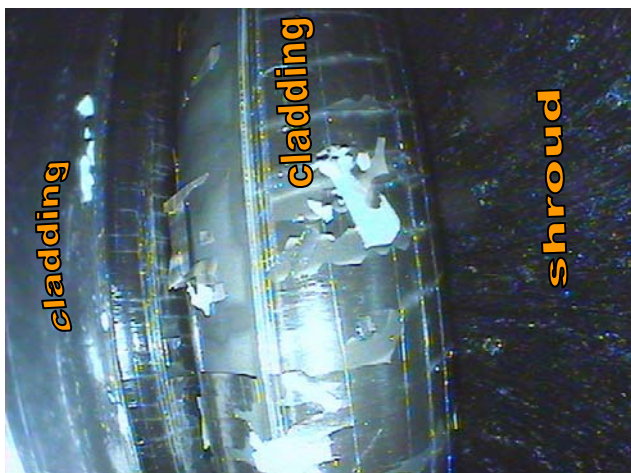


Fig. 8. Videoscope photograph with a side-view lens at elevation 0.40 m: dark inner oxide sub-layer at cladding surface.

Most of the debris due to oxide scale spalling accumulated at the bottom of the bundle (Fig. 11) and at the upper edge of spacers.



Fig. 9. Videoscope photograph with a side-view lens at elevation of 0.70 m: intensive oxide scale spalling on the coarse shroud surface.



Fig. 10. Videoscope photograph at elevation of 0.90 m: circumferential and longitudinal cracks at the cladding; nodular breakaway corrosion at the shroud.

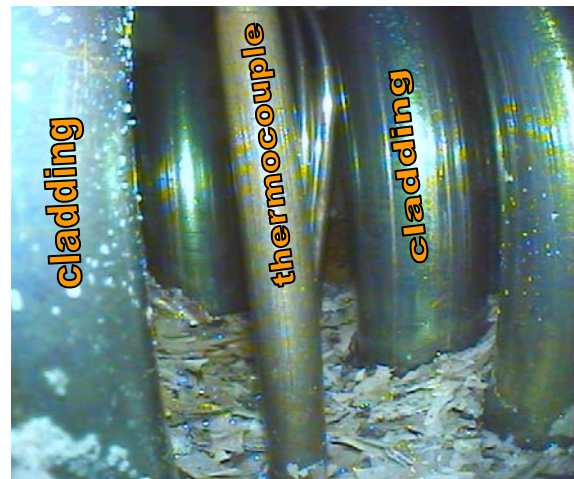


Fig. 11. Spalled oxide scales as debris at the bundle bottom.

V. METALLOGRAPHIC EXAMINATION

The preparation of the bundle for metallographic investigation was performed with its encapsulation into epoxy resin. After hardening of the resin, the bundle was sawn into cross-section slabs, which were subjected to metallographic analysis⁵. The mechanisms of the physical-chemical interaction of the components and of their oxidation are deduced, paying special attention to the cladding oxidation.

Overview of top side of the cross-section from elevation 0.55 m is depicted in Fig. 12. This surface corresponds to upper edge of the third grid spacer. Very many rubble fragments can be distinguished, obviously collected on top of the spacer grid. The relocated rubble consists of partial cladding scale shells and fragments of partially oxidized cladding.



Fig. 12. Cross section overview at 0.55 m elevation.

Fig. 13 illustrates the cladding oxidation of the central rod. An earlier grown partial layer of the scale tends to spall from a thicker next one which is found split from the α -Zr(O) layer.

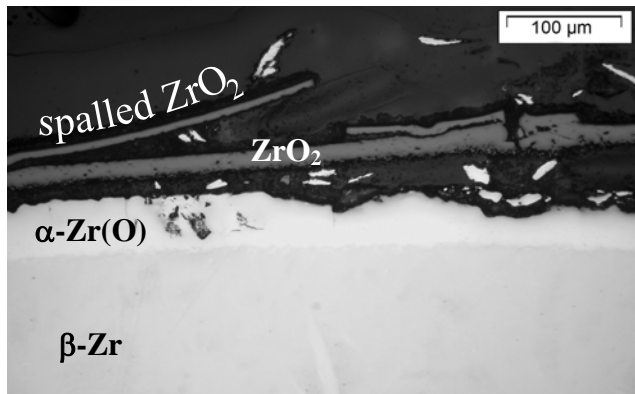


Fig. 13. Oxidation of the central rod at elevation 0.55 m: spalling of oxide scales due to breakaway effect

At the given elevation (0.55 m) the temperatures during the pre-oxidation period were about 1050 K, which is the lowest value of the breakaway range for the E110 alloy⁴. But the temperature rise from 1050 K to 1200 K during the transient test phase was not sufficient to leave the breakaway regime later on. For the other upper elevations the typical breakaway temperatures were experienced mainly during the pre-oxidation period.

In order to take into account the breakaway loss of scales for the elevations 0.55, 0.65, 0.75, 0.85 and 0.115 m, an evaluation of thickness measurement results for the simulator rods was performed. A calculated average oxide layer thickness for the respective elevations was gained as follows. Subtraction of the measured average remaining metal thickness value from the original tube wall thickness, nominally 700 μm , gives the consumed metal thickness. Multiplication of this by the Pilling-Bedworth factor 1.56 gives the corresponding calculated oxide layer thickness, used as basis for quantification of the lost partial scale thickness in addition to that of the measured remaining scale (Fig. 14).

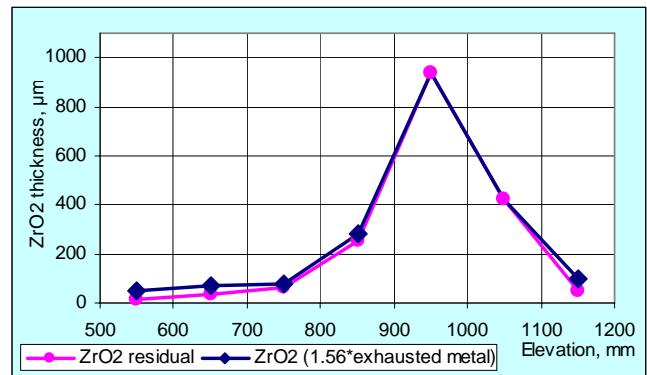


Fig. 14. Cladding oxidation: measured residual oxide and oxide calculated on the base of residual metal.

The pronounced breakaway effect at elevations 0.55 m, 0.65 m, 0.105 m provoked much more intensive original bundle oxidation in comparison to reference test QUENCH-06. Indeed the estimated total oxide layer thickness at elevations 0.55 m was about $80 \pm 11 \mu\text{m}$ for QUENCH-12 and only $20 \pm 1 \mu\text{m}$ for QUENCH-06. The high scatter in QUENCH-12 was due to the relatively large lateral temperature differences in this test.

The melting temperature of the cladding alloy matrix ($> 1900 \text{ K}$) was exceeded at elevation 0.95 m. Fig. 15 gives an impression of the bundle degradation state at this elevation. On the one hand the cladding oxidation and the cladding brittleness are much more advanced than at the adjacent elevations. On the other hand there are several rod groups, which are bound together in clusters due to formation of common melt pools. Neck formation between rods and parts of the inner shroud structure took place.



Fig. 15. Cross section overview at 0.95 m elevation.

An example of such a melt pool is depicted in Fig. 16. Some metallic melt remains at rods 8 and 31, whereas most of the cladding of rod 19 rod is fully oxidized. The rounded shape of voids indicates loss of melt by downward relocation. The other part of released metallic melt, enclosed by rods 8, 31, and 19, is captured within the triangular space between the claddings. The embedded oxide scale segments have been thinned by oxygen transfer to the melt from outer and inner side.

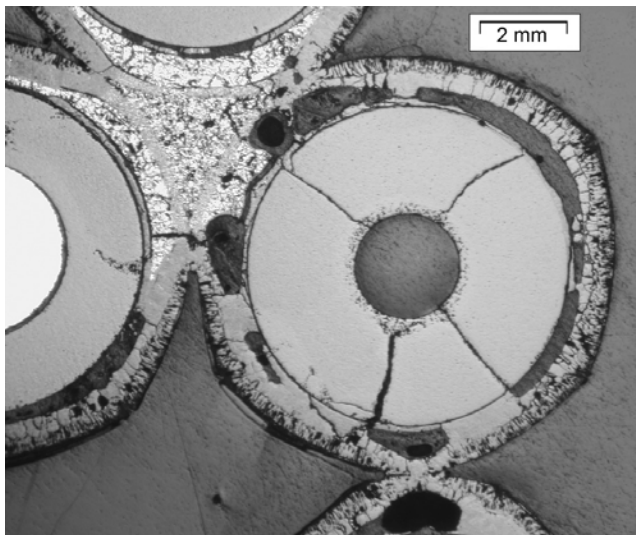


Fig. 16. Melt pool formation via necking mechanism

The relatively large oxidised melt fraction was not observed in QUENCH-06. This should be taken into account when comparing the hydrogen releases.

VI. HYDROGEN UPTAKE AND PRODUCTION

Hydrogen uptake by the corner rods was measured by neutron radiography at PSI. The hydrogen content in the corner rods reached a maximum of 35 at% at the bundle elevation of about 1.10 m (Fig. 17).

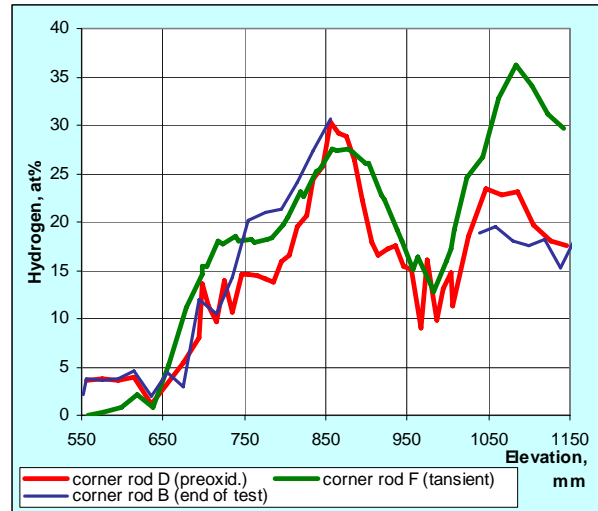


Fig. 17. Hydrogen uptake by the corner rods obtained by neutron radiography.

Measurements of hydrogen production are as follows: 34 g were released during the pre-oxidation and transient phases and about 24 g in the quench phase. The amount released in the quench phase is six times higher than in QUENCH-06 with ~4 g (Fig. 18). The reasons for the increased hydrogen production may be extensive damaging of the cladding surfaces due to the breakaway oxidation, local melt formation with subsequent melt oxidation, and a release of previously picked-up hydrogen.

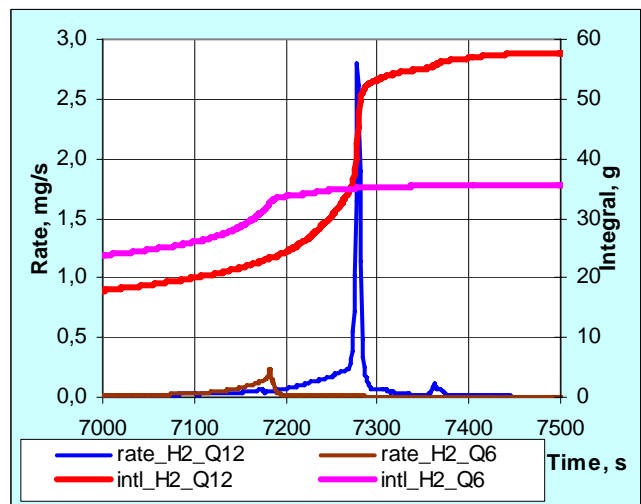


Fig. 18. Comparison of hydrogen release during QUENCH-12 and QUENCH-06.

VII. POST-TEST CALCULATION RESULTS

Preliminary post-test calculations were performed using local versions of SCDAP/RELAP5, following on from pre-test analyses⁶ in support of the test definition. The starting point for the input model used for QUENCH-12 (Q-12) simulation was evolved from post-test analyses of previous QUENCH tests. Extensive changes were made to accommodate the Q-12 bundle configuration, and provisional values were assumed for the additional resistance based on measurements made prior to the test. View factors amongst the rods were modified for hexagonal bundle geometry, based on calculations by Vasiliev⁷. A correlation⁸ for Zr-1%Nb (E110) oxidation kinetics was incorporated into a local version of the code to indicate how the new material might affect the oxidation. To the extent that the two correlations are believed to reflect the oxidation rates of the respective cladding materials, the Cathcart-Pawel (C-P)/Urbanic-Heidrick (U-H) model, for Zry-4, can be thought of as a corresponding to a QUENCH-06 (Q-06) counterpart with the Q-12 bundle geometry, while the one using the E110 correlation corresponds to Q-12 itself. A second local code version incorporated the high temperature Prater-Courtright (P-C) oxidation correlation in the form recommended by Schanz⁹.

Since the code input was extensively revised from those used for all previous QUENCH experiments, it was benchmarked using results of the Q-12 pre-test trial. Following the comparison, a small adjustment was made to the additional electrical resistance in the heater rod model and the model was then used for the final prediction of Q-12. The same input was denoted as the base model for the present post-test calculations following minor changes in the boundary conditions to reflect the actual test procedure. The condition used for quench initiation was defined as follows. For the case using the E110 correlation, the timing was advanced by 50 s from the experimental value so that the calculated temperature at 0.95 m corresponded to the quench initiation criterion of 2073 K. To facilitate model-model comparison, the same timing was used in the calculations with the other oxidation correlations. The results described below focus mainly on the “base” calculation made with identical boundary conditions and with each of the three code versions.

As a preliminary, supporting calculations were also performed with various slightly adjusted end conditions and using SCDAPSIM, all with the E110 correlation. Fig. 19 compares the axial temperature profiles from those complementary calculations at a time shortly before quench initiation, with the measured data. In fact the cases are rather similar, the main difference occurring towards to top and bottom of the bundle. The agreement is excellent at 0.95 m but with some distortion of the profile.

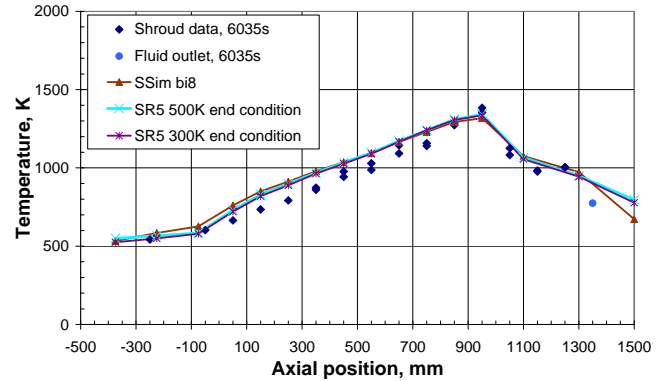


Fig. 19. Axial temperature profile on shroud.

Figs. 20 and 21 compare the results using the three correlations with the measured temperatures at the hottest elevation (0.95 m) of the central rod and shroud, respectively. All of the cases are close to the data during the plateau, with almost perfect agreement with the E110 correlation and only a very slightly higher temperature with Cathcart-Pawel. The E110 correlation leads to a sharper increase than U-H during the transient phase just before quench initiation, but with little impact on the temperature at that time. P-C gives a large overestimate in temperature just prior to quench. However, all three cases exhibit rapid cooling and quenching at almost the same time. The results for bundle refilling and quench progression for the E110 case are compared with the data in Fig. 22, while the other cases are somewhat similar. The time offset is due to the 50 s earlier quench initiation adopted in the calculation. The observed water ingress during the fast refill phase is typical of QUENCH experiments but is not calculated. The slow-down of the refill and quenching above 0.95 m is explained by the breach in the shroud which had occurred already at that elevation.

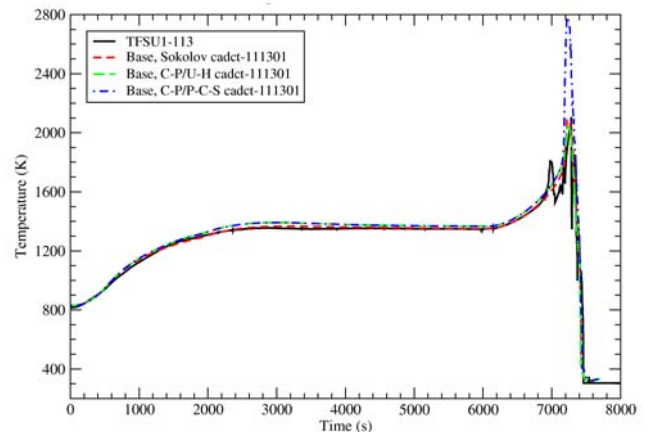


Fig. 20. Temperature at 0.95 m elevation on central rod.

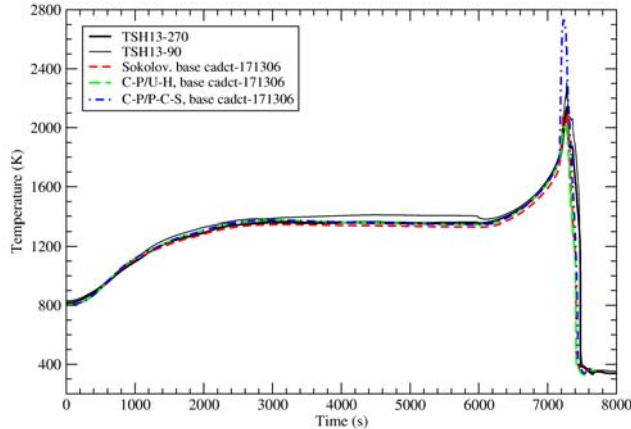


Fig. 21 Temperature at 0.95 m elevation on shroud.

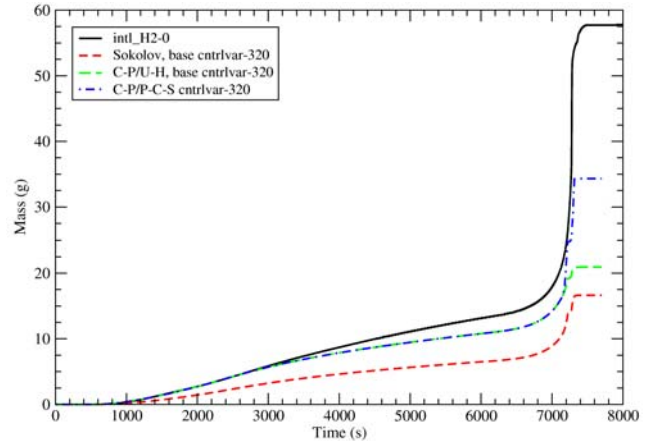


Fig. 23. Calculated and measured hydrogen generation.

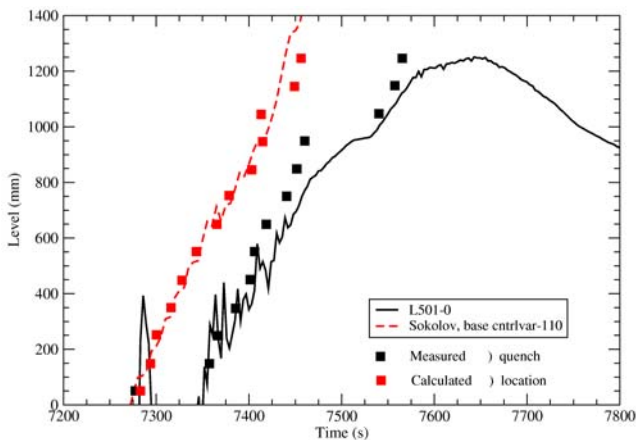


Fig. 22. Calculated and measured liquid level and quench progression.

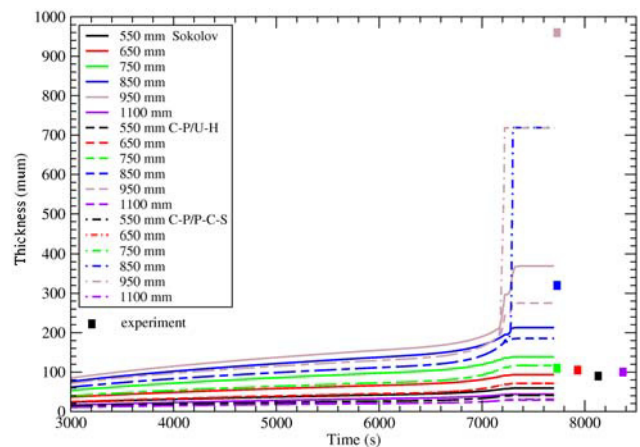


Fig. 24. Calculated and measured oxide scale thickness.

Despite the similar thermal response through almost the entire sequence, all of the calculations underestimated the oxidation, as can be seen in Fig. 23. The E110 correlation gives a much lower hydrogen generation during the plateau phase of the experiment, although the final mass is similar to the C-P/U-H case due to greater oxidation just before and during quench. The C-P/P-C correlation gives the closest agreement for hydrogen mass, including a significant oxidation during quench, but the rate is overestimated in the period just before while the total mass is still underestimated overall.

Although the E110 correlation gives a lower oxidation rate than C-P/U-H, the oxide thickness is greater. In fact the correlations for oxidation rate and oxide thickness are derived separately from weight gain and scale thickness measurements. The thicker oxide scale calculated by the E110 correlation suggests an inconsistency with the oxidised mass, or else evidence of a very low oxide density. Even so, Fig. 24 shows an underestimate over most of the oxidised length.

It is worthwhile to consider the calculated oxidation in relation to a comparison between Q-06 and Q-12. The pre-quench phases of Q-12 yielded 34 g, compared with 32 g in Q-06. The effect of cladding material cannot be assessed by directly comparing the Q-06 and Q-12 results, partly because of the greater oxidisable surface area in Q-12 (*1.22), and partly because the pre-oxidation plateau temperatures were up to 100 °C lower in Q-12. After taking into account the area ratio, the pre-quench oxidation in Q-12 is only slightly less than Q-06, despite the lower temperatures. In fact, although analyses of Q-06^{2,10} showed the C-P correlation to give quite good agreement for the pre-quench hydrogen generation, both the Sokolov and C-P correlation give an underestimate for Q-12. These considerations suggest that the E110 cladding is more susceptible to oxidation than Zry-4, as could also be expected from the observed breakaway. The quench phase of Q-12 yielded 24 g of hydrogen, which was much more than in Q-06. The correlations all significantly underestimate the quench oxidation in Q-12, even the C-P/P-C model which strongly overestimated both the oxidation kinetics and the temperatures just before the start of quench. The differences between the correlations

therefore do not explain the much greater hydrogen generation. Instead it appears this was due to processes outside the frame of a parabolic kinetic treatment, which enhanced the oxidation. In Q-12 but did not occur in Q-06. Indeed, the QUENCH experiments have shown that hydrogen generation during reflood is a strong cliff-edge effect, triggered by various possible factors including the onset of metallic melting. A recent analysis by Vasiliev¹⁰ identifies a number of factors that may have contributed to the reflood oxidation during Q-12. Faster kinetics at temperatures above 1600 °C or more extensive shattering of the oxide scale cannot be ruled out. However, the analysis indicates that the metallic melting observed at some locations may be a more likely cause.

VIII. CONCLUSIONS

The QUENCH-12 experiment was carried out to investigate the effects of VVER materials and bundle geometry on core reflood, in comparison with the test QUENCH-06 (ISP-45) with western PWR geometry.

During the pre-oxidation and transient phases the E110 cladding alloy is susceptible to breakaway oxidation within relative broad temperature range (1050 – 1300 K). Oxide scale of layered type showed spalling into sub-layers and loss of fragments, which were collected at spacer grids and bundle bottom.

At the peak temperature elevation of 0.95 m, melt pool formation, non-coherent melt relocation, dissolution of embedded scale and melt oxidation were observed.

The total hydrogen production was 58 g (QUENCH-06: 36 g), 24 g of which were released during reflood (QUENCH-06: 4 g).

The S/R5 code adequately reproduced the QUENCH-12 thermal transient. Both the C-P and Sokolov correlations underestimated the oxidation kinetics, but preliminary analysis indicates that the comparison with QUENCH-06 is consistent with the change in the bundle configuration and cladding material; in particular breakaway effects may have enhanced the oxidation. None of the models captured the greater oxidation during reflood in QUENCH-12, possibly due to exposure of molten metallic to the steam.

Further assessment and possible revision of the Sokolov correlation is recommended, using new data being generated from experiments at FZK and elsewhere.

ACKNOWLEDGMENTS

The FZK work is sponsored by the HGF Programme NUKLEAR. The PSI analysis is supported by funds provided by Swissnuclear, and by the European Commission 6th Framework Network of Excellence, SARNET, Contract FI6O-CT-2004-509065.

NOMENCLATURE

E110	Russian cladding alloy Zr1%Nb
FZK	Forschungszentrum Karlsruhe
HGF	Helmholtz-Gemeinschaft Deutscher Forschungszentren
PSI	Paul Scherrer Institute
PWR	Pressurised Water Reactor
VVER	Vodo-Vodyanoi Energetichesky Reactor (PWR of Russian type)

REFERENCES

1. J. STUCKERT et al., "Results of the QUENCH-12 Experiment with a Russian VVER-type Bundle", FZKA 7307 (2008).
2. L. SEPOLD et al., "Experimental and Computational Results of the QUENCH-06 test (OECD ISP-45)." FZKA 6664, 2004.
3. L. YEGOROVA et al., "Experimental Study of Embrittlement of Zr-1%Nb VVER Cladding under LOCA-Relevant Conditions." NUREG/IA-0211, 2005
4. M. STEINBRÜCK, "Oxidation of Advanced Zirconium Alloys in Oxygen in the Temperature Range 600-1600 °C". 16th Int. Conf. on Nuclear Engineering (ICONE16), Orlando, Florida, May 2008.
5. G. SCHANZ, U. Stegmaier, M. Heck, J. Stuckert. "Post-Test Examination of the WVER Bundle QUENCH-12". 13th Int. QUENCH Workshop, FZ Karlsruhe, Germany (2007).
6. J. BIRCHLEY, T. Haste, W. Hering and C. Homann, "Pre-test Analytical Support for Experiments QUENCH-10, -11 and -12", Int. Conf. Nuclear Energy for New Europe 2006, Portorož, Slovenia (2006).
7. A. VASILIEV, IBRAE Moscow, unpublished (2006).
8. N. B. SOKOLOV, L. N. Andreeva-Andrievska, V. Yu. Vlasov et al., "Genetics of the Interaction of VVER Reactor Core Materials – Recommendations for Use on the Basis of the International Standard Problem on the CORA-W2 Experiment", A A Bochvar All-Russian Scientific Research Institute for Inorganic Materials (VNIINM) Report N8068, Moscow, Russia (1993).
9. A. VOLCHEK, Y. Zvonarev and G. Schanz, "Advanced Treatment of Zircaloy Cladding High Temperature Oxidation in Severe Accident Calculations PART II. Best-fitted parabolic correlations", Nuc. Eng. Des. 232, 85-96 (2004).
10. A. VASILIEV, "QUENCH-12 versus QUENCH-06 Comparative Calculation Analysis using SOCRAT 1.1 Code", 13th Int. QUENCH Workshop, FZ Karlsruhe, Germany (2007).